**Proceedings of the REHVA Annual Meeting Conference**
**Low Carbon Technologies in HVAC**
**23 April 2018, Brussels, Belgium**

https://www.rehvam2018atic.eu/

# MODELING AND EXPERIMENTAL RESULTS OF A RESIDENTIAL HEAT PUMP WITH VAPOR INJECTION AND VARIABLE SPEED SCROLL COMPRESSOR

**Bertrand Dechesne[1*], Vincent Lemort[1]**

[1] Thermodynamics Laboratory, University of Liège, Belgium, bdechesne@ulg.ac.be

## ABSTRACT

The market share of heat pump systems has grown significantly in Europe in the past decades and, in residential applications, air-source heat pumps (ASHP) are usually considered due to their relatively low cost. In the literature, it has been widely demonstrated that injection cycle can improve the system performance and operating range. This paper presents an experimental study and a compressor model of such a system.

The first part of the paper focus on the experimental results collected from a vapor injection and variable speed scroll compressor air-to-water residential heat pump. The unit is a 10kW residential system working with R410a as working fluid and capable of providing floor heating and domestic hot water. It was tested in a controlled environment in order to achieve a wide range of outdoor and indoor conditions. The impact of the split lines and of the four-way valve on the superheat level is described. Finally, the impact on the system performance of the levels of superheat of both injection and suction ports is discussed.

The second part of this paper presents a model of the variable speed compressor. A thermodynamic model of the vapor injection scroll compressor is developed using empirical correlations for the volumetric efficiency, isentropic efficiency and the ratio between the injection and suction mass flow rates.

Finally, the comparison between the compressor model predictions and results from a steady-state experimental campaign is given.

**KEY WORDS:** Injection heat pump, variable speed, scroll compressor, experimental, modeling.

## 1. INTRODUCTION

In residential applications, air-source heat pumps (ASHP) are usually considered due to their relatively low cost. Improving performances of ASHP has been a major concern in the last decades and one option is the use of variable speed compressor and vapor injection. [1] gave a deep literature review on the later option comparing the different injection options and focusing both on the system level and the components level. [2] compared different advanced vapor compression cycle technologies (such as expander cycle, ejector, etc) and showed that, taking into account the performances of these systems as described in the literature, the vapor injection cycle is one the most promizing technology. [3] compared different architectures of injection cycle and although the economizer architecture does not show the best performances, it has the advantage to be easier to control than flash tank architecture.

This paper presents experimental results of an air source heat pump (ASHP) using a variable speed vapor injection scroll compressor and R410A as working fluid. The impact of the superheat levels on the system performances is investigated and the control issues are discussed. An empirical model of the vapor injection

*Corresponding Author: bdechesne@uliege.be

scroll compressor is developed using empirical correlations for the volumetric efficiency, isentropic efficiency and the ratio between the injection and suction mass flow rates.

## 2. EXPERIMENTAL INVESTIGATIONS

This section aims at presenting the experimental set-up used in these investigations as well as the main results that were obtained.

The studied system is a residential air-to-water heat pump. It is a split system working with a variable speed scroll compressor with vapor injection. An internal heat exchanger (i.e. economizer) is used to evaporate the refrigerant stream that is injected in the scroll during the compression process. Split lines are present between the two units and can measure up to 25m. The drive cooler is a small heat exchanger made up of an aluminium plate in contact with both refrigerant tubes and the drive electronic circuit in order to cool down the latter (c.f. Fig. 1).

### 2.1 Experimental set-up

The set-up is schematized in Fig. 1.

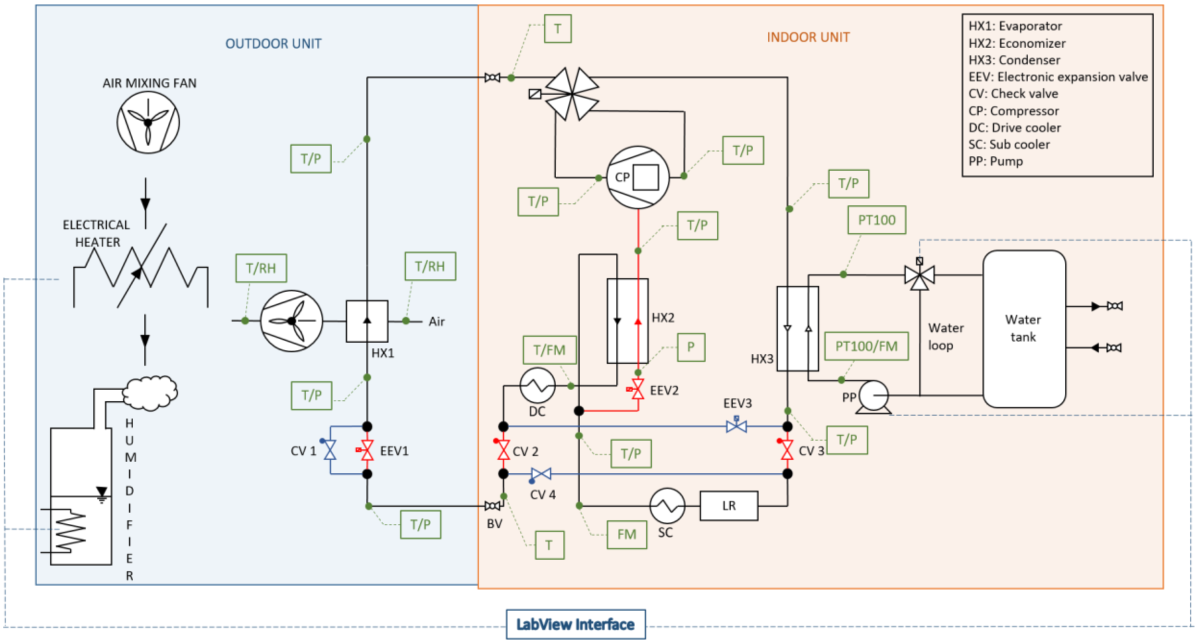


**Fig. 1** Experimental set-up scheme.

The refrigerant loop is controlled by means of a ModBus Interface, which implies the adjustment of the rotational speed of the air evaporator fan, of the scroll compressor, the openings of the expansion valves as well as the four-ways valves. An additional heat exchanger, called drive cooler, is installed to cool down the power electronic used for the variation of the compressor speed.

Conditions in terms of temperature and absolute pressure are measured at the supply/exhaust of each component of the refrigerant loop. Temperatures are determined by means of sensor pockets (type T thermocouple) with accuracy of ±0.3 K. Used absolute pressure sensors show the following characteristics:

- Operating range of 0-20 bar for the sensor used at the supply of the compressor with an accuracy of 1% of the full scale range;

- Operating range of 0-30 bar for sensors used for measuring the low and intermediate pressure level with an accuracy of ±1% of the full scale range;
- Operating range of 0-50 bar for sensors used for measuring the high pressure with an accuracy of ±0.5% of the full scale range.

Water flow rate passing through the condenser is controlled by adjusting the rotational speed of the water pump. The water temperature at the supply of the condenser can be controlled using a valve and tap water. Given the low temperature difference between the supply and the exhaust of the condenser (between 3 and 10K), PT100 with accuracy of ±0.1 K have been preferred instead of type T thermocouple. Water flow rate is determined by means of an impulse water meter (4 pulses per liter).

**Table 1** List of sensors and related accuracy.

| Sensors | Error |
|---|---|
| Type T thermocouples | ±0.3 K |
| PT100 class 1/10 DIN | ±0.1 K |
| Keller 0-20 bar absolute pressure | ±0.2 bar |
| Keller 0-30 bar absolute pressure | ±0.3 bar |
| Keller 0-50 bar absolute pressure | ±0.25 bar |
| Siemens SITRANS differential pressure | ±0.05 mbar |
| Krohne Optimass 6000 | ±0.1 % |
| Emerson micro-motion CMF025 | ±0.1 % |
| Impulse water meter | 4 pulses per liter |
| Power meter | |

The outdoor unit is installed in a room where conditions are controlled in terms of both humidity and temperature. Relative humidity is controlled by the use of electrical steam generators (humidifier). It is also possible to control with precision the outdoor air temperature by means of a set of variable electrical resistances. The relative humidity at the inlet and at the outlet of the outdoor air stream passing through the air evaporator are measured by means of relative humidity sensors with an accuracy of ± 1.5 percent points.

## 2.2 Superheat analysis

Tests were carried out at constant speed and steady working conditions in order to investigate the impact of the superheat levels on the system performances. Results for 3000 RPM, 0°C outside temperature and 55°C water inlet temperature are presented in Fig. 2. First of all, at time t=0, it can be seen that the superheat level at the exhaust of the evaporator and the suction port of the compressor is quite different. This is mainly due to the heat transfer in the four-way valve.

In phase I (time ∈ [0; 1500[), the outdoor valve opening is increased in order to reduce the superheat at the exhaust of the evaporator down to 5K. The coupled problem of superheat control is shown during this phase. In fact, the injection superheat increases during this phase even though the injection expansion valve opening has remained constant. This is due to a higher mass flow rate on the high pressure side of the economizer because of the increased outdoor valve opening. At the end of phase 1, the COP has increased from 2.25 to 2.54 while the heating capacity has increased by 16%. On the other end, the discharge temperature dropped from 115.3 to 110.3°C. These values have been averaged over 300 seconds.

In a second phase (time ∈ [1500; 2500]), the injection expansion valve opening is increased in order to bring the level of superheat back to 5K. It can be seen that no coupling occurs this time, i.e., the control of the injection expansion valve does not affect significantly the outdoor level of superheat. Decreasing the level of superheat on the injection line increase the amount of injected refrigerant and helps to increase by 3 additional percent the heating capacity compared to the end of phase I. The discharge temperature is also decreased to 102.9°C but the COP remains approximately constant compared to the end of previous phase (2.56).

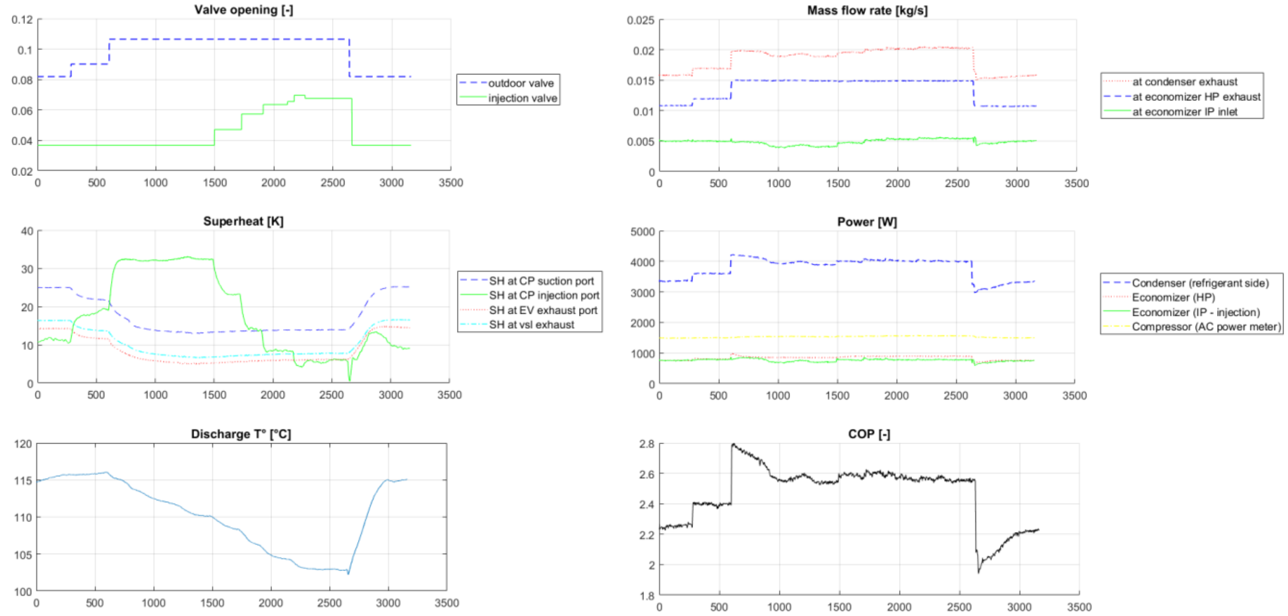


**Fig. 2** Experimental results for superheat analysis at constant working conditions (3000 RPM, 0°C outdoor temperature and 50°C water supply temperature to the condenser).

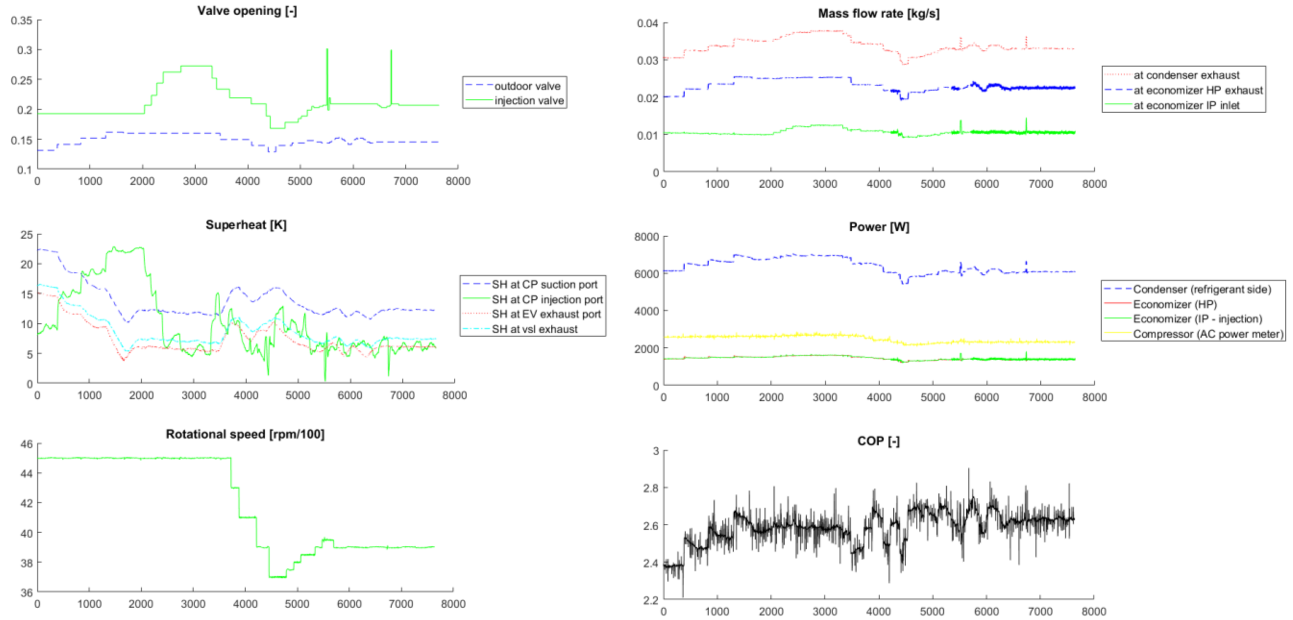


**Fig. 3** Experimental results for superheat analysis with speed decrease to maintain equal heating capacity.

In Fig. 3, the same test was carried out at 4500 RPM and for an outdoor temperature of 7°C. The water supply temperature was set to 55°C. However, a third phase (time ∈ [3800; 7500]) was added in order to compare system performance for a constant heating capacity. It can be concluded that a better control of both level of superheat helped to decrease the rotational speed by more than 10% and the discharge temperature by 12.5K and increase the COP from 2.38 to 2.63 at constant heating capacity.

Tab. 2 gives an overview of the COP, discharge temperature and heating capacity evolution at the beginning of the test, the end of phase 1 and 2 for different working conditions.

**Table 2** COP, discharge temperature and heating capacity variation at the beginning of each test, end of phase I and II for several working conditions.

| N | $T_{out}$ | $T_{water}$ | COP | | | $\Delta\dot{Q}_{cd}$ [%] | | | $T_{dis}$ [°C] | | |
|---|---|---|---|---|---|---|---|---|---|---|---|
| rpm | °C | °C | $t_0$ | I | II | $t_0$ | I | II | $t_0$ | I | II |
| 3000 | 0 | 50 | 2.25 | 2.54 | 2.56 | 0 | 16.0 | 19.0 | 115 | 110 | 103 |
| 4500 | 0 | 50 | 2.24 | 2.50 | 2.55 | 0 | 14.5 | 19.4 | 120 | 112 | 106 |
| 6000 | 0 | 50 | 2.16 | 2.34 | 2.36 | 0 | 11.7 | 14.4 | 124 | 120 | 113 |
| 4500 | 7 | 55 | 2.38 | 2.57 | 2.58 | 0 | 11.7 | 14.4 | 118 | 113 | 106 |
| 6000 | 7 | 55 | 2.26 | 2.39 | 2.38 | 0 | 7.7 | 10.2 | 123 | 114 | 106 |

## 3. MODELING

A compressor model is presented in this section. This model can be integrated in a system dynamic model developed in the Modelica language in order to be able to develop and test advanced controller [4].

### 3.1 Compressor

The proposed model uses a set of five dimensionless polynomials to predict the compressor behavior. The inputs of the compressor polynomials are the rotational speed $N_{rot}$ and both total and injection pressure ratios, i.e.

$$r_{p,tot} = \frac{P_{ex}}{P_{su}} \tag{1}$$

$$r_{p,inj} = \frac{P_{inj}}{P_{su}} \tag{2}$$

Both mass flow rates, exhaust state and compressor consumption can be computed thanks to the five polynomials which are the volumetric and isentropic effectiveness ($\varepsilon_v$ and $\varepsilon_s$), the drive efficiency ($\eta_{drive}$), the injection ratio ($X_{inj}$) and the ambient losses ratio ($X_{loss}$). Finally, the model can be written as follows:

$$\dot{M}_{su} = \varepsilon_v \,.\rho_{su} \,.V_s .N \tag{3}$$

$$\dot{M}_{inj} = X_{inj} \,.\dot{M}_{su} \tag{4}$$

$$\dot{W}_{in} = \frac{\dot{W}_s}{\varepsilon_s} \tag{5}$$

$$\dot{W}_s = \dot{M}_{su} \,.\left(h_{ex,s} - h_{su}\right) + \dot{M}_{inj} \,.\left(h_{ex,inj,s} - h_{inj}\right) \tag{6}$$

$$\dot{W}_{el} = \frac{\dot{W}_{in}}{\eta_{drive}} \tag{7}$$

$$\dot{Q}_{loss} = \dot{W}_{in} \cdot X_{loss} \tag{8}$$

Where $\dot{W}_{in}$ is the electrical power delivered to the compressor motor and $\dot{W}_s$ the isentropic power. This latter is composed of two terms related to the isentropic compression of two separate volumes performing the compression process from the suction to the discharge pressure for the first one and from the injection to the discharge pressure for the second one. The five dimensionless polynomials are of the form:

$$\varepsilon_v = a_0 + a_1\, r_{p,tot} + a_2\, N \tag{9}$$

$$X_{inj} = b_0 \ln(b_1\, r_{p,inj}) \tag{10}$$

$$\varepsilon_s = \frac{c_0 \exp\left(-c_1 * \left(r_{p,tot} - c_2\right)\right)}{1 + \exp\left(-c_3 * \left(r_{p,tot} - c_2\right)\right)} \tag{11a}$$

$$with\ c_i = c_{i,0}\left(1 + c_{i,1}\frac{N}{N_{max}} + c_{i,2}\left(\frac{N}{N_{max}}\right)^2\right), \forall\, i \in [0;3] \cap Z \tag{11b}$$

$$\eta_{drive} = d_0 + d_1\, N + d_2\, N^2 + d_3\, N^3 \tag{12}$$

$$X_{loss} = e_0 \tag{13}$$

The form of Eq. 11a is based on [5]. This model was calibrated with steady-state experimental data collected on the test bench described in previous section. A total of 27 steady-state points, all across the compressor operating map were used (cf. Tab. 3). The condensing and evaporating temperature are defined for a quality of 1 and respectively the pressure at the condenser inlet and at the evaporator exhaust.

**Table 3** Testing conditions ranges

| Variables | Min. Value | Max Value |
|---|---|---|
| Compressor speed [rpm] | 2000 | 7000 |
| Water inlet temperature [°C] | 17.6 | 62.8 |
| Water temperature increase [K] | 2.0 | 9.4 |
| Outside air temperature [°C] | -15.9 | 45.9 |
| Condensing temperature [°C] | 20.1 | 65.0 |
| Heating capacity [W] | 3000 | 12700 |
| Evaporating temperature [°C] | -24.3 | 24.8 |

The parity plots of the main outputs are given in Fig. 4 and the model parameters are presented in Tab. 4.

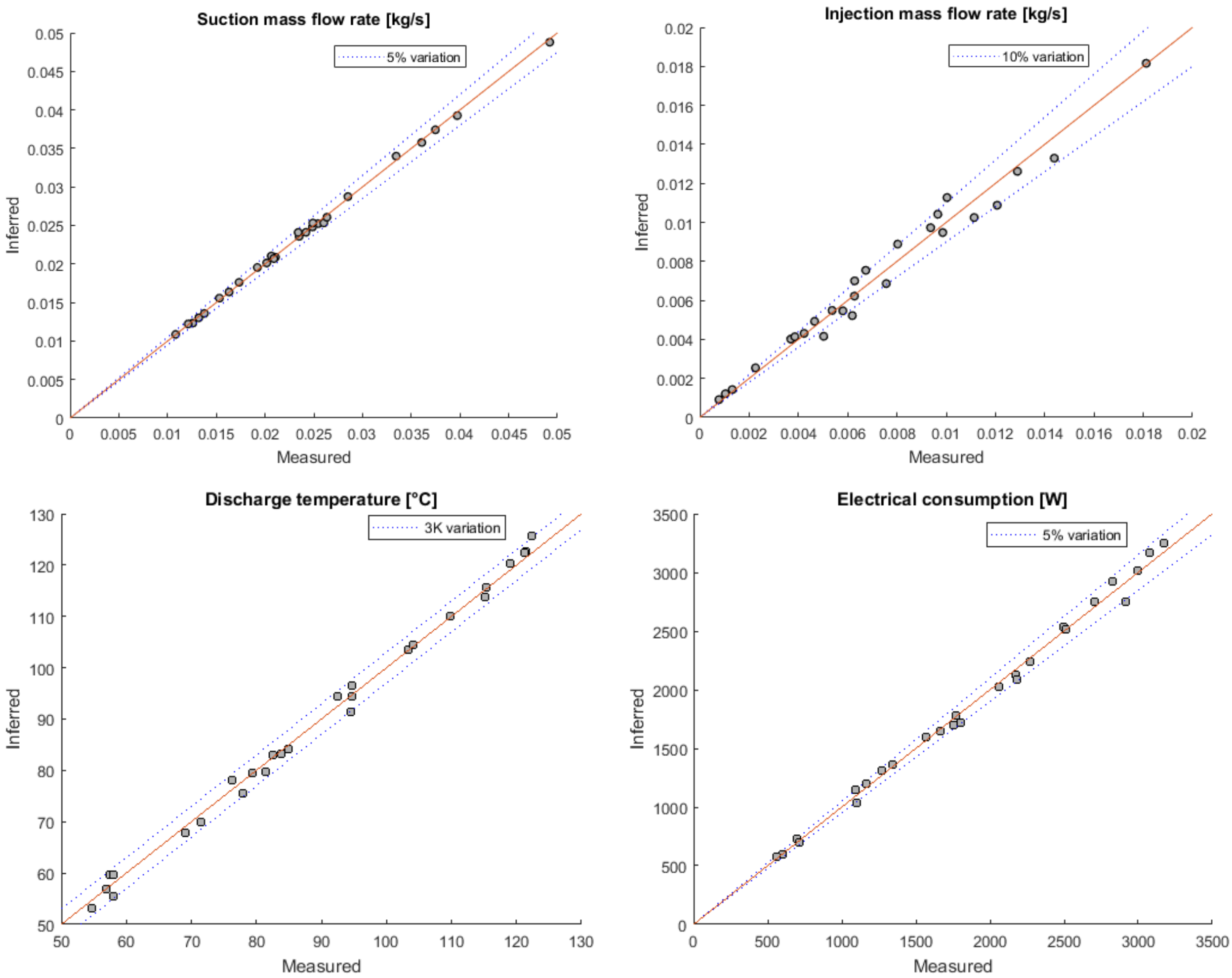


**Fig. 4** Compressor model parity plots.

**Table 4** Compressor model parameters

| Parameters | 1 | 2 | 3 | 4 | 5 | 6 |
|---|---|---|---|---|---|---|
| $a_i$ | 0.9622 | -0.01622 | 7.445E-06 | - | - | - |
| $b_i$ | 1.091 | 0.6694 | - | - | - | - |
| c_0 | 0.544 | 1.217 | -0.979 | - | - | - |
| $c_{1,i}$ | 0.04797 | -0.2836 | - | - | - | - |
| $c_{2,i}$ | 1.006 | 0.2555 | - | - | - | - |
| $c_{3,i}$ | 2.021 | - | - | - | - | - |
| $d_i$ | 0.8553 | 4.701E-05 | -7.506E-09 | 4.074E-13 | - | - |
| $e_i$ | 0.0975 | - | - | - | - | - |

The shape of the isentropic efficiency curve is given in Fig. 5. This curves takes into account efficiency decrease due to over or under-compression and the impact of the rotational speed.

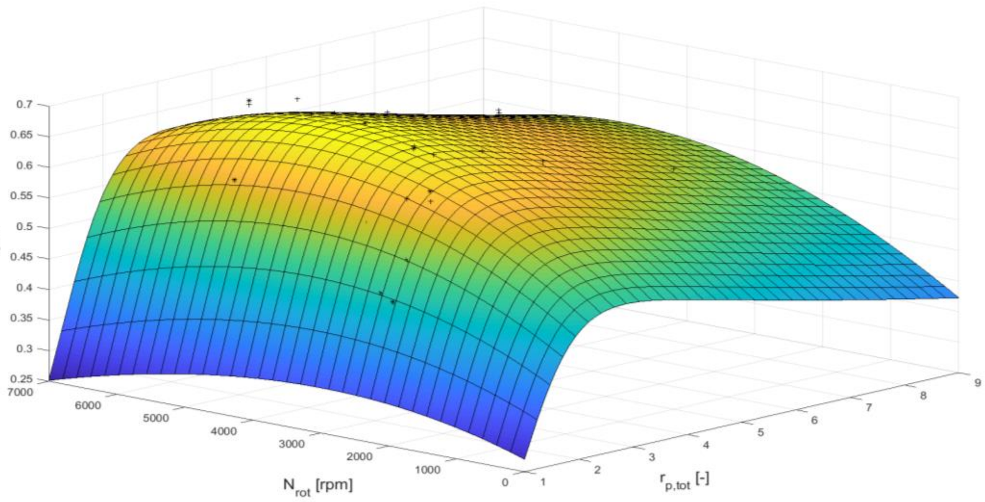


**Fig. 5** Isentropic efficiency surface.

## 4. CONCLUSIONS

The impact of the superheat control on the heat pump performance was presented in this paper. It was first shown that the four-way valve has a significant impact on the level of superheat at the suction port of the compressor. In fact, this component behaves as a small heat exchanger between the high pressure hot gases and the colder, low pressure, gases entering the compressor. Moreover, the coupling of the superheat control for both the suction and injection superheat was presented. This exhibits the need of advanced control for this kind of system as simple SISO PID controller are not optimal. A possible solution would be the use of a static decoupler as presented in [6]. Furthermore, it was shown for different working conditions that the level of superheat has a significant impact on the system performance. The COP and heating capacity can be increased by about 10 and 15% while the discharge temperature is decreased by more than 10K if the superheat level are decreased from 15 to 5K.

Finally, an empirical model of the compressor was proposed and showed good prediction results for the electrical consumption, both mass flow rates and the discharge temperature despite a relative simplicity and low-order of the polynomials. This model can be integrated in a dynamic model of the system in order to test or develop advanced control. Moreover, the polynomials used in the model are dimensionless, hence, this model could be used for any compressor size [7].

## REFERENCES

[1] Xu, Xing, Yunho Hwang, and Reinhard Radermacher. "Refrigerant injection for heat pumping/air conditioning systems: literature review and challenges discussions." *International Journal of Refrigeration* 34.2 (2011): 402-415.

[2] Park, Chasik, et al. "Recent advances in vapor compression cycle technologies." *International Journal of Refrigeration* 60 (2015): 118-134.

[3] Heo, Jaehyeok, et al. "Comparison of the heating performance of air-source heat pumps using various types of refrigerant injection." *International Journal of Refrigeration* 34.2 (2011): 444-453.

[4] Dechesne, Bertrand, et al. "Comparison of a dynamic model and experimental results of a residential heat pump with vapor injection and variable speed scroll compressor." *PROCEEDINGS OF ECOS 2017* (2017).

[5] Underwood, C. P., M. Royapoor, and B. Sturm. "Parametric modelling of domestic air-source heat pumps." *Energy and Buildings* 139 (2017): 578-589.

[6] Astrom, Karl Johan, Karl Henrik Johansson, and Qing-Guo Wang. "Design of decoupled PID controllers for MIMO systems." *American Control Conference, 2001. Proceedings of the 2001*. Vol. 3. IEEE, 2001.

[7] Dechesne, Bertrand, and Stéphane Bertagnolio. "Empirical model of a variable speed vapor injection compressor for air source heat pump dynamic modeling." *International conference on compressors and their systems*. 2015.